

AG-VPReID.VIR: Bridging Aerial and Ground Platforms for Video-based Visible-Infrared Person Re-ID

Huy Nguyen, Kien Nguyen, Akila Pemasiri, Akmal Jahan, Clinton Fookes, and Sridha Sridharan
 School of Electrical Engineering and Robotics, Queensland University of Technology
 {nguyet91, k.nguyenthanh, a.thondilege, akmal.jahan, c.fookes, s.sridharan}@qut.edu.au

Abstract

Person re-identification (Re-ID) across visible and infrared modalities is crucial for 24-hour surveillance systems, but existing datasets primarily focus on ground-level perspectives. While ground-based IR systems offer nighttime capabilities, they suffer from occlusions, limited coverage, and vulnerability to obstructions—problems that aerial perspectives uniquely solve. To address these limitations, we introduce AG-VPReID.VIR, the first aerial-ground cross-modality video-based person Re-ID dataset. This dataset captures 1,837 identities across 4,861 tracklets (124,855 frames) using both UAV-mounted and fixed CCTV cameras in RGB and infrared modalities. AG-VPReID.VIR presents unique challenges including cross-viewpoint variations, modality discrepancies, and temporal dynamics. Additionally, we propose TCC-VPReID, a novel three-stream architecture designed to address the joint challenges of cross-platform and cross-modality person Re-ID. Our approach bridges the domain gaps between aerial-ground perspectives and RGB-IR modalities, through style-robust feature learning, memory-based cross-view adaptation, and intermediary-guided temporal modeling. Experiments show that AG-VPReID.VIR presents distinctive challenges compared to existing datasets, with our TCC-VPReID framework achieving significant performance gains across multiple evaluation protocols. Dataset and code are available at <https://github.com/agvpred25/AG-VPReID.VIR>.

1. Introduction

Person re-identification (Re-ID) aims to match images or videos of individuals captured across different cameras, times, or viewpoints. It has become a crucial task in computer vision with applications in surveillance and security systems [32, 44]. Traditional Re-ID methods focus on matching RGB images obtained from ground-based cameras under well-lit conditions [20, 16]. However, real-world surveillance scenarios often involve varying illumination

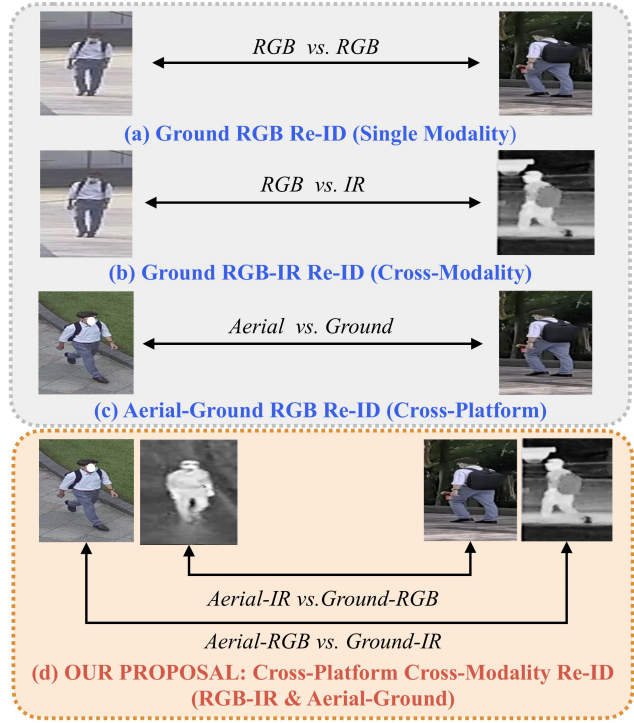


Figure 1. Existing person Re-ID works mainly focus on ground-based setting, either (a) single-modality RGB vs. RGB or (b) cross-modality RGB vs. IR. Recent advances in aerial-ground Re-ID only operate in (c) single-modality RGB vs. RGB. We propose a new cross-platform cross-modality setting (d) for person Re-ID.

conditions, including low-light or nighttime environments, where RGB cameras may fail to capture useful information [34, 18]. In such cases, infrared (IR) imaging provides a viable solution due to its ability to capture images in low-light conditions [4, 17].

Within person Re-ID, several works have explored the aerial-ground setting [24, 26]. Nguyen et al. [25] introduced AG-ReID.v2 with 100,502 RGB images of 1,615 identities, while Zhang et al. [47] proposed G2A-VReID with 185,907 video frames from 2,788 identities. However, both operate exclusively in RGB modality. Despite

significant progress in cross-modality Re-ID for ground-based cameras, the combination of aerial-ground perspectives with RGB-IR modalities remains unexplored.

Cross-modality person Re-ID, particularly between RGB and IR images, has attracted significant interest for enabling 24-hour surveillance by bridging the day-night gap [34, 18]. Several datasets have been proposed for cross-modality Re-ID, such as SYSU-MM01 [34], RegDB [23], HITSZ-VCM [18], and BUPTCampus [6]. However, these datasets primarily focus on ground-based surveillance and do not consider the cross-modality scenario for aerial-ground setting, which is critical for comprehensive surveillance systems involving both UAVs and ground cameras.

To address these limitations, we introduce AG-VPReID.VIR, a novel aerial-ground cross-modality video-based person Re-ID dataset. This dataset extends existing datasets by incorporating both RGB and IR modalities captured from aerial and ground perspectives. The combined challenges of cross platforms (aerial vs. ground) and cross modalities (RGB vs. IR) presents unique challenges to be addressed. The dataset contains 4,861 tracklets from 1,837 identities, captured by multiple UAV-mounted and fixed CCTV cameras in both modalities. This diverse collection presents unique challenges including cross-viewpoint variations, modality discrepancies, and temporal dynamics, making it a valuable benchmark for developing robust Re-ID systems. Fig. 1 illustrates our proposed dataset and its differences compared to previously proposed settings.

Furthermore, we propose TCC-VPReID (Three-stream architecture for Cross-platform Cross-modality Video-based Person Re-ID), a novel architecture specifically designed for RGB-IR aerial-ground person Re-ID. Our approach aims to effectively leverage both spatial and temporal information while addressing the significant domain gaps between aerial-ground views and RGB-IR modalities. Through extensive experiments on AG-VPReID.VIR, we demonstrate that our method achieves superior performance compared to existing state-of-the-art approaches.

The main contributions of this work are: (1) We introduce the first aerial-ground cross-modality video-based person Re-ID dataset, enabling research into more practical surveillance systems; (2) We establish baseline performance metrics through comprehensive benchmarking of state-of-the-art approaches; (3) We develop TCC-VPReID, a three-stream architecture that is purposely designed to address aerial-ground viewpoint variations and RGB-IR modality discrepancies through style-robust feature learning, memory-based cross-view adaptation, and temporal modeling. The dataset, baseline models, and our approach will be made publicly available.

Table 1. Comparison of AG-VPReID.VIR with other person re-identification datasets.

Dataset	View & Modality				Statistics		
	Ground		Aerial		#IDs	#Tracklets	#Frames
Image-based Datasets							
AG-ReID.v2 [25]	✓	-	✓	-	1,615	-	100,502
RegDB [23]	✓	✓	-	-	412	-	8,240
SYSU-MM01 [34]	✓	✓	-	-	491	-	303,420
LLCM [48]	✓	✓	-	-	1,064	-	46,767
Video-based Datasets							
G2A-VReID [47]	✓	-	✓	-	2,788	5,576	180,000
HITSZ-VCM [18]	✓	✓	-	-	927	21,863	463,259
BUPTCampus [6]	✓	✓	-	-	3,080	16,826	1,869,366
AG-VPReID.VIR (Ours)	✓	✓	✓	✓	1,837	4,861	124,855

2. Prior Work

Visible-Infrared Person Re-ID Datasets: RGB-IR person re-identification has gained interest for 24-hour surveillance. SYSU-MM01 [34] pioneered with 491 identities across 6 cameras, while RegDB [23] provided 412 identities with paired RGB-thermal images. Video-based datasets emerged with HITSZ-VCM [18] (927 identities, 463,000 frames) and BUPTCampus [6] (3,080 identities, 1.87 million frames). However, these datasets focus solely on ground-level perspectives, lacking the aerial viewpoints crucial for comprehensive surveillance. Table 1 and Fig. 2 compare our proposed dataset with other visible-infrared datasets.

Aerial-Ground Person Re-ID Datasets: Aerial-ground perspectives in Re-ID research emerged with AG-ReID.v2 [25] (100,502 RGB images, 1,615 identities) and G2A-VReID [47] (185,907 video frames, 2,788 identities). However, these datasets only include visible spectrum imagery, limiting nighttime utility. Our dataset uniquely combines aerial and ground views in both modalities for robust Re-ID across varied lighting and viewpoints.

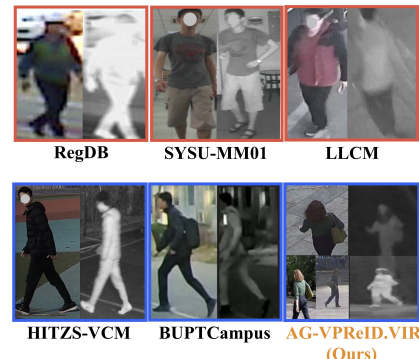


Figure 2. Our visible-infrared images vs. existing datasets' visible-infrared images. Red border indicates image-based vs. blue border indicates video-based setting.

Visible-Infrared Person Re-ID: Cross-modality person Re-ID methods fall into two main approaches: learning modality-shared features through specialized architectures [41, 40], and employing adversarial learning [4, 33] to align

feature distributions between modalities. Most existing methods assume identical data distributions between training and testing phases—an assumption that does not hold in practical Re-ID scenarios with non-overlapping identity sets. Additionally, these methods primarily consider images from similar ground-level perspectives, overlooking significant viewpoint variations. Our work specifically addresses the joint challenges of cross-modality and cross-platform variations, which represent a significant gap in existing literature.

Video-based Person Re-ID: Video-based person Re-ID methods extract temporal information through three primary approaches: recurrent neural networks [22, 38, 21] for sequential dependency modeling, temporal pooling operations [38, 3, 37] for frame-level feature aggregation, and 3D convolutions [15, 10, 21] for direct spatio-temporal pattern extraction. Recent advances include spatial-temporal memory networks [7, 18, 6] that store representations of spatial distractors and temporal patterns. While these methods have shown success in single-domain settings, they typically address either cross-modality challenges [18, 6] or cross-viewpoint variations [47] in isolation. Our work aims to overcome these unprecedented domain gaps through a novel architecture optimized for aerial-ground RGB-IR video-based Re-ID.

3. AG-VPReID.VIR dataset

3.1. Dataset Collection

The AG-VPReID.VIR dataset was collected at a university campus using a combination of UAVs, stationary CCTV cameras, and wearable devices. Inspired by a previously published dataset [25], which included RGB images from UAVs, CCTV, and wearable cameras, AG-VPReID.VIR enhances data diversity by integrating IR images captured from UAVs and CCTV cameras equipped with thermal sensors. This addition allows for comprehensive surveillance capabilities under various lighting conditions, particularly in low-light or nighttime environments where RGB cameras are less effective.

For the UAV platform, we employed DJI M600 Pro drones equipped with dual-sensor cameras capable of capturing synchronized RGB and IR images. The UAVs were operated at altitudes ranging from 15 to 45 meters to capture individuals from elevated perspectives with varying resolutions and scales. For ground-level surveillance, we utilized two CCTV cameras, comprising a standard visible-light (RGB) camera and a thermal imaging (IR) camera. The wearable devices provide ground-level RGB images from first-person viewpoints. Table 2 provides detailed specifications of our camera setup. Camera locations and view coverage are presented in the Appendix Sec. 7.

The data collection was conducted over five months,

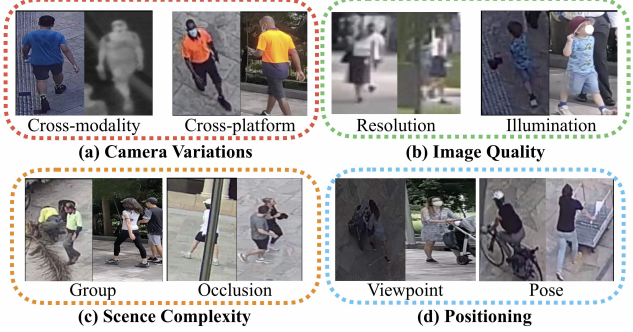


Figure 3. Challenges in our proposed dataset.

comprising 10 distinct sessions. During each session, UAV flights were performed at multiple altitudes (15m, 25m, and 45m), with each flight lasting 15 minutes to ensure comprehensive coverage. We gathered a total of 124,855 images of 1,837 unique identities. The AG-VPReID.VIR dataset includes both RGB and IR images captured across different camera modalities and perspectives. The inclusion of IR imagery significantly enhances the dataset’s applicability for person re-identification tasks under varied environmental conditions.

Table 2. Camera specifications used in data collection.

Device	Mod.	Brand	Model	Res.	FPS	Alt.
CCTV	RGB	Bosch	N/A	704×480	15	≈3m
Wearable	RGB	Vuzix	M4000	4K	30	≈1.5m
UAV	RGB	DJI	XT2	3840×2160	30	15~45m
UAV	NIR	DJI	XT2	640×512	30	15~45m
CCTV	NIR	Avigilon	N/A	800×600	30	≈4m

3.2. Labeling Process

To ensure accurate cross-modal and cross-platform person re-identification, each individual in the dataset was manually annotated with a unique identity label consistent across RGB and IR images, as well as across UAV, CCTV, and wearable camera views. Initially, the YOLOv10x (Ultralytics) detector with pretrained weights as the backbone [13] were employed for person detection and tracking, extracting frames at regular intervals. Annotators manually reviewed the automatically detected tracks to correct any inaccuracies, ensuring that each tracklet corresponds to a single individual across all modalities and platforms. This two-stage process ensures high-quality annotations while maintaining efficiency in the labeling workflow.

The final dataset contains 124,855 images corresponding to 1,837 unique identities captured across 5 camera views. The labeling process accounted for challenges such as varying image resolutions, significant viewpoint differences, and modality discrepancies between RGB and IR images. Multiple annotators cross-verified the labels to enhance annotation accuracy. The dataset distribution analysis is presented in Appendix Sec. 8.

3.3. Dataset Characteristics

The AG-VPReID.VIR dataset exhibits several unique characteristics compared to existing RGB-IR person re-identification datasets such as RegDB [23], SYSU-MM01 [34], HITSZ-VCM [18], and BUPTCampus [6]. Table 1 provides a comparative overview of these datasets. The key characteristics of the AG-VPReID.VIR dataset include:

- **Unique Multi-Platform Multi-Modal Integration:** Unlike existing datasets, which either capture only ground-based RGB-IR data (SYSU-MM01, RegDB, HITSZ-VCM, BUPTCampus) or only RGB data across aerial-ground platforms (AG-ReID.v2, G2A-VReID), our dataset uniquely incorporates both RGB and IR modalities from both aerial and ground-based cameras, providing the first comprehensive cross-platform cross-modality collection for person Re-ID.
- **Unique Aerial IR:** Our dataset is the first to introduce IR images from UAV platforms for person ReID. As shown in Fig. 3(a), aerial IR images are very challenging compared to Ground IR images, posing interesting challenges for the research community to address.
- **Novel Viewpoint and Scale Challenges:** The dataset captures individuals from various angles and distances, resulting in significant variations in appearance and scale. Due to different camera heights and types, UAV-captured images range from 31×59 to 371×678 pixels, while ground-based images span from 22×23 to 172×413 pixels, as illustrated in Fig. 3(a) and Fig. 3(b).
- **Other Challenges:** In addition, our dataset poses various challenges existing in person Re-ID including scene complexity with partially occluded subjects and individuals walking in groups as depicted in Fig. 3(c), and positioning challenges from different viewpoints and poses as presented in Fig. 3(d).

3.4. Ethics and Privacy

This study was conducted with full ethical approval from the institutional review board. All participants provided informed consent prior to data collection. To protect privacy, we employed the “Deface” [5] for facial anonymization, implemented secure data storage protocols with restricted access, and established clear guidelines for responsible data usage.

4. Our Method

We propose TCC-VPReID, a novel three-stream framework purposely designed to address the unique challenges of cross-platform cross-modality person re-identification.

In particular, our approach is designed with complementary techniques to handle (1) the style variations and appearance distortions across platforms (*Stream 1*), (2) the temporal and cross-view challenges of video-based (*Stream 2*) and (3) the modality gap challenges between visible and infrared domains (*Stream 3*). Fig. 4 illustrates our architecture, highlighting three specialized streams and the feature fusion module that preserves complementary information while reconciling contradictions across platforms and modalities.

4.1. Stream 1: Style-Robust Feature Learning

To overcome the dramatic style variations and appearance distortions across aerial-ground platforms and RGB-IR modalities, our first stream implements a novel style-robust feature extraction mechanism. While inspired by recent style augmentation techniques [51], we significantly extend this approach with platform-specific style transformations tailored to the unique characteristics of aerial and ground perspectives.

This stream generates diverse training representations by strategically varying input frame styles:

$$I_t^{aug} = [\alpha I_t^R, \beta I_t^G, \gamma I_t^B], \quad (1)$$

$$I_t^{ir,aug} = \delta I_t^{ir}, \quad (2)$$

where I_t and I_t^{ir} denote the t -th RGB and infrared frames, respectively. I_t^R, I_t^G, I_t^B represent the red, green, and blue channels of I_t , and α, β, γ , and δ are sampled from a uniform distribution $U(0.5, 1.5)$ as proposed in [51].

Our innovation lies in developing a cross-platform defense mechanism that maintains feature consistency despite the extreme viewpoint and modality variations. We employ strategically placed intra-modal style attacks between network’s convolutional blocks:

$$\tilde{f}_{conv3}^{i,j} = \frac{\sigma(f_{conv3}^{k,l})}{\sigma(f_{conv3}^{i,j})} \cdot (f_{conv3}^{i,j} - \mu(f_{conv3}^{i,j})) + \mu(f_{conv3}^{k,l}), \quad (3)$$

where $f_{conv3}^{i,j}$ denotes the feature from the third convolutional block for the i -th identity and j -th frame, $f_{conv3}^{k,l}$ represents a feature from a different identity-frame pair (k,l) selected for disturbance, and $\sigma(\cdot)$ and $\mu(\cdot)$ represent the variance and mean operations on the input feature. This approach forces the model to develop viewpoint-invariant and modality-invariant representations through our specialized optimization objective:

$$L_{SA} = L_{dis} + L_{con}, \quad (4)$$

where L_{dis} enforces identity consistency through cross-entropy loss and L_{con} enforces feature consistency through the distance between original and attacked features.

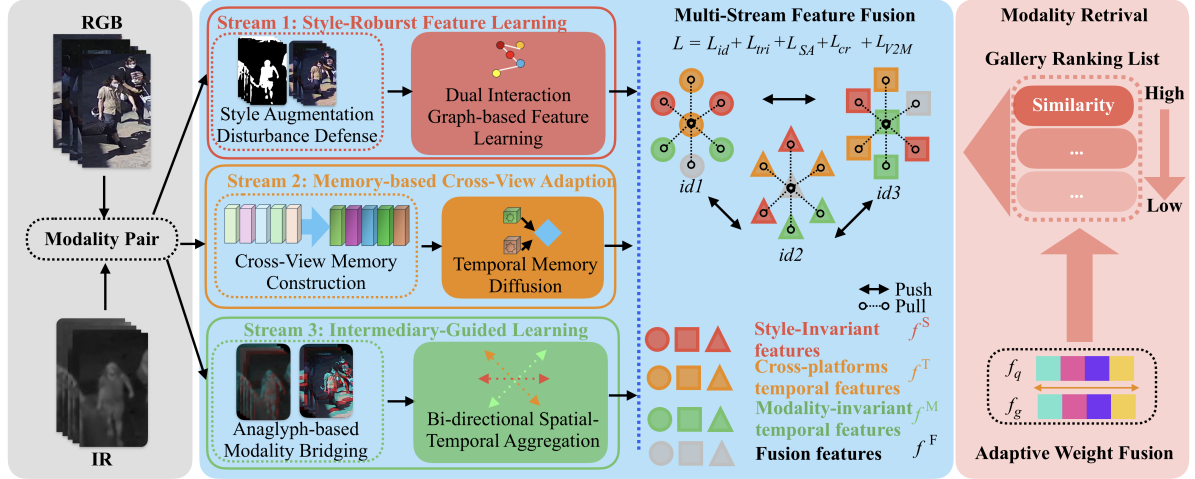


Figure 4. Overview of our proposed three-stream architecture: (1) Style-Robust Stream for handling appearance variations via style augmentation and graph learning; (2) Memory-based Cross-View Stream for bridging aerial-ground perspectives; and (3) Intermediary-Guided Temporal Stream for addressing RGB-IR modality gaps. These streams combine in a fusion module for effective cross-platform, cross-modality person re-identification.

4.2. Stream 2: Memory-based Cross-View Adaptation

The dramatic geometric and perspective changes between aerial and ground viewpoints represent one of the most challenging aspects of cross-platform Re-ID. Our second stream introduces a novel memory-based architecture that explicitly models and bridges these viewpoint differences through tailored representation learning and adaptive cross-view alignment.

The centerpiece of our innovation is the development of specialized view-specific memory representations [46, 50, 1] that separately model aerial and ground viewpoints:

$$M_{y_i}^{aerial} = \frac{1}{N_i^{aerial}} \sum_{v_a \in y_i^{aerial}} v_a, \quad (5)$$

$$M_{y_i}^{ground} = \frac{1}{N_i^{ground}} \sum_{v_a \in y_i^{ground}} v_a, \quad (6)$$

where $M_{y_i}^{aerial}$ and $M_{y_i}^{ground}$ are the memory representations for identity y_i from aerial and ground views respectively, v_a represents a sequence-level feature vector extracted from the visual encoder, N_i^{aerial} and N_i^{ground} represent the number of aerial and ground sequences for identity y_i , respectively. Unlike traditional approaches that use a single global memory per identity, our dual-memory architecture explicitly captures the distinct characteristics of each viewing angle.

We further introduce a cross-platform attention mechanism that dynamically updates each memory type:

$$M_{y_i}^{m'} = \mathcal{P}_{y_i}^m + M_{y_i}^m, \quad (7)$$

where $m \in \{aerial, ground\}$ denotes the platform type, $M_{y_i}^{m'}$ is the updated memory representation, and $\mathcal{P}_{y_i}^m$ is a platform-specific prompt generated via a dual-branch attention-based decoder that explicitly shares information across platforms while preserving platform-specific characteristics.

Our innovative video-to-memory contrastive loss optimizes these representations:

$$L_{V2M}(y_i) = -\frac{1}{|P(y_i)|} \sum_{p \in P(y_i)} \log \frac{\exp(v_p \cdot M_{y_i}^{m'}/\tau)}{\sum_{j=1}^B \exp(v_j \cdot M_{y_i}^{m'}/\tau)}, \quad (8)$$

where $P(y_i)$ represents all positive samples for identity y_i in the batch, v_p is the feature vector of a positive sample, v_j refers to the feature vector of the j -th sample in the batch, τ is a temperature parameter, and B is the batch size.

4.3. Stream 3: Intermediary-Guided Temporal Learning

The fundamental domain gap between visible and infrared modalities presents unique challenges, particularly when coupled with aerial-ground viewpoint variations. Our third stream introduces a novel intermediary-guided temporal learning module specifically designed to bridge these modality differences while preserving critical identity information.

Our core approach generates modality-invariant anaglyph representations via edge detection [14]:

$$a(i, j) = \sum_m \sum_n x(i+m, j+n) A(m, n) + k, \quad (9)$$

where $a(i, j)$ is the (i, j) -th pixel of anaglyph image a , $x(i, j)$ represents the original image (RGB or IR), $A(m, n)$ denotes an edge detection operator with indices $m, n \in \{-1, 0, 1\}$, and k is an offset value.

Our innovation lies in the development of a specialized 3D cross-attention mechanism that strengthens modality-invariant information while preserving spatial-temporal patterns critical for aerial-ground alignment. This is complemented by our cross-reconstruction constraint that explicitly minimizes the modality gap:

$$L_{cr} = \sum_{t=1}^{b \times k} \|a_t^v - R(a_t^{ir})\|_2 + \sum_{t=1}^{b \times k} \|a_t^{ir} - R(a_t^v)\|_2, \quad (10)$$

where a_t^v and a_t^{ir} represent anaglyph features from visible and infrared data respectively, R denotes a reconstruction network consisting of convolutional layers, b is the mini-batch size, and k is the number of frames in each video clip. This approach forces the model to learn modality-invariant features that are robust to the dramatic appearance differences between RGB and IR data.

4.4. Multi-Stream Integration and Loss Functions

The three streams provide complementary information for cross-platform cross-modality person re-identification. We integrate these streams through a feature fusion module and optimize using a joint loss function:

$$L_{total} = L_{id} + \lambda_1 L_{tri} + \lambda_2 L_{SA} + \lambda_3 L_{cr} + \lambda_4 L_{V2M}, \quad (11)$$

where hyperparameters $\lambda_1, \lambda_2, \lambda_3$, and λ_4 balance the contribution of each loss term from the three streams described earlier. During inference, the fused feature serves as the final person representation for cross-domain matching, with adaptive weighting applied to each stream's contribution based on validation performance.

5. Experimental Results

5.1. Datasets and Evaluation Metrics

For a thorough evaluation, we validate our approach on two established visible-infrared benchmarks HITSZ-VCM [18] and BUPTCampus [6]. We also conduct comprehensive experiments on our AG-VPReID.VIR dataset. As shown in Table 3, we maintain a strict separation between training and testing identities, with 326 IDs (978 tracklets, 24,793 frames) reserved for training and the remaining identities used for testing across four challenging evaluation scenarios: ground-to-ground, aerial-to-aerial, ground-to-aerial, and aerial-to-ground. Each protocol includes both visible-to-infrared (V2I, where visible images serve as queries and IR images as gallery) and infrared-to-visible (I2V, where IR images serve as queries and visible images as gallery) matching directions. For I2V experiments, we further increase the difficulty by introducing additional distractor identities in the gallery set, creating a more realistic

surveillance scenario with 1,184 distractor IDs contributing 30,532-34,687 frames depending on the platform. We adopt standard person Re-ID evaluation metrics: Cumulative Matching Characteristic (CMC) along with mean Average Precision (mAP) [6, 45] to comprehensively measure retrieval performance across all ranking positions.

Table 3. Train/test statistics for AG-VPReID.VIR. Q=Query, G=Gallery. V2I: visible to infrared, I2V: infrared to visible.

Set	Platforms	Modalities	# IDs	# Tracklets (Q/G)	# Frames (Q/G)
Training	All	–	326	978	24,793
Testing	Ground to Ground	V2I	199	313/199	9,357/3,018
		I2V*	199	199/313	3,018/9,357
	Aerial to Aerial	V2I	174	174/174	6,284/3,115
	Aerial to Aerial	I2V*	174	174/174	3,115/6,284
Testing	Ground to Aerial	V2I	116	184/116	5,360/1,701
		I2V*	260	260/260	3,530/10,939
Testing	Aerial to Ground	V2I	260	260/260	10,939/3,530
		I2V*	116	116/184	1,701/5,360

* For all I2V experiments, 1,184 additional distractor IDs are added to the gallery set.

5.2. Implementation Details

Our TCC-VPReID framework uses PyTorch on an NVIDIA A100 GPU. The three streams include: (1) Style-Robust stream with ResNet50 [11] using style augmentation from $U(0.5, 1.5)$ and adaptive instance normalization; (2) Memory-based stream with CLIP ViT-B/16 [28] encoder and a 2-layer transformer decoder [30]; (3) Intermediary-Guided stream with a dual-branch architecture using anaglyph data and bidirectional LSTMs [21]. These backbones and network architectures were selected based on the best performing models in the respective papers [51, 45, 14]. Training uses Adam optimizer (initial $lr=3.5 \times 10^{-4}$) with cosine annealing. Each batch contains 8 identities \times 4 sequences \times 8 frames. Model trains for 120 epochs with hyperparameters $\lambda_1 = 1.0$, $\lambda_2 = 1.5$, $\lambda_3 = 1.0$, and $\lambda_4 = 1.5$ (see Appendix Sec. 10).

5.3. Comparison with State-of-the-Art Methods

We evaluate our method against state-of-the-art approaches on HITSZ-VCM, BUPTCampus, and AG-VPReID.VIR datasets. We focus on ground-to-ground evaluation (Table 4) for fair comparison, with cross-platform ablations in Tables 5 and 6.

Performance on Existing Datasets. On HITSZ-VCM, our method achieves 72.16%/56.43% (Rank-1/mAP) for I2V and 75.92%/57.84% for V2I, outperforming SAADG by 2.94%/2.66% and 2.79%/1.75%. On BUPTCampus, we reach 69.73%/67.25% for I2V and 68.47%/65.38% for V2I, exceeding AuxNet by 3.25%/3.14% and 3.24%/3.19%.

Performance on AG-VPReID.VIR. Our method shows the most significant gains on AG-VPReID.VIR, where we achieve 36.18%/41.56% for I2V and 46.33%/59.23% for

Table 4. Comprehensive Comparison of Cross-Modal Person Re-Identification Methods.

Method	Venue	Ground \leftrightarrow Ground								Ground \leftrightarrow Ground					
		HITSZ-VCM				BUPTCampus				AG-VPReID.VIR					
		I2V		V2I		I2V		V2I		I2V		V2I			
Image-based Methods															
AlignGAN [31]	ICCV'19	42.15	27.43	44.62	29.73	27.99	30.32	35.37	35.13	4.12	6.32	3.94	8.21		
LbA [27]	ICCV'21	46.38	30.69	49.30	32.38	32.09	32.93	39.07	37.06	5.23	7.14	4.82	9.43		
MPANet [36]	CVPR'21	46.51	35.26	50.32	37.80	33.45	34.17	40.56	38.22	5.94	8.21	5.63	10.55		
SPOT [2]	TIP'22	52.23	37.10	53.67	38.96	37.52	38.24	44.12	41.03	7.32	9.87	6.42	11.63		
HCT [19]	TMM'20	55.39	38.62	57.25	39.73	38.92	39.47	45.62	42.18	7.83	10.54	7.21	12.37		
DDAG [43]	ECCV'20	54.62	39.26	59.03	41.50	40.44	40.86	46.30	43.05	8.12	11.25	7.83	13.42		
MMN [49]	MM'21	53.24	39.82	56.43	41.47	40.86	41.71	43.70	42.80	7.95	11.08	7.42	13.15		
CAJL [42]	ICCV'21	56.59	41.49	60.13	42.81	40.49	41.46	45.00	43.61	9.12	12.86	8.76	15.32		
VSD [29]	CVPR'21	54.53	41.18	57.52	43.45	41.27	42.05	47.84	44.63	8.45	12.03	8.12	14.27		
AGW [44]	TPAMI'21	47.23	36.12	51.85	38.50	36.38	37.36	43.70	41.10	6.74	9.23	6.17	11.08		
DEEN [48]	CVPR'23	65.32	50.16	68.42	50.83	49.81	48.59	53.70	50.43	11.23	16.45	10.54	19.23		
SGIEL [8]	CVPR'23	67.65	52.30	70.23	52.54	48.32	47.15	51.42	49.27	12.43	17.92	11.21	20.45		
Video-based Methods															
TCLNet [12]	ECCV'20	48.32	36.45	52.13	38.52	37.15	36.87	41.32	38.92	9.23	12.54	8.37	15.76		
CAViT [35]	ECCV'22	54.83	40.26	58.18	41.63	42.63	41.87	46.52	43.15	10.45	14.83	9.72	17.63		
DART [39]	CVPR'22	62.85	44.26	63.92	46.43	52.43	49.10	53.33	50.45	11.56	15.82	10.23	18.76		
MITML [18]	CVPR'22	63.74	45.31	64.54	47.69	49.07	47.50	50.19	46.28	12.16	16.93	10.87	19.42		
AuxNet [6]	TIFS'23	51.05	45.99	54.58	48.70	66.48	64.11	65.23	62.19	15.70	16.46	12.89	22.57		
CST[9]	TMM'24	69.44	51.16	72.64	51.16	54.92	52.87	56.35	53.26	14.23	19.37	12.64	22.05		
IBAN [14]	TCSVT'23	65.03	48.77	69.58	50.96	53.42	51.36	54.17	52.43	6.03	9.46	3.83	10.16		
SAADG [51]	ACM MM'23	69.22	53.77	73.13	56.09	55.76	53.42	57.83	54.82	13.07	18.75	11.82	21.14		
Ours	-	72.16	56.43	75.92	57.84	69.73	67.25	68.47	65.38	36.18	41.56	46.33	59.23		

Table 5. Comprehensive Results on Cross-Platforms Cross-Modal AG-VPReID.VIR Dataset.

Method	Aerial \rightarrow Ground								Ground \rightarrow Aerial											
	I2V				V2I				I2V				V2I							
	R1	R5	R10	R20	mAP	R1	R5	R10	R20	mAP	R1	R5	R10	R20	mAP	R1	R5	R10	R20	mAP
St1	7.76	17.24	22.41	35.34	9.54	7.31	23.46	39.62	52.31	17.46	12.31	26.54	40.00	47.69	20.64	14.13	27.72	44.02	57.61	23.05
St2	11.21	28.45	36.21	45.69	17.68	40.38	70.77	82.69	92.31	54.40	27.31	52.69	63.08	71.92	39.27	27.17	50.54	65.76	79.35	39.25
St3	2.59	11.21	17.24	22.41	4.86	5.38	13.46	22.69	36.92	11.50	3.08	14.23	18.46	26.92	9.10	7.07	20.65	33.15	47.28	15.61
St12	15.52	31.90	43.10	51.72	20.91	46.92	77.31	86.15	92.31	59.71	34.23	56.54	70.77	78.85	45.62	30.43	56.52	67.39	80.98	42.45
St13	9.48	18.97	28.45	37.93	10.94	8.08	26.15	41.92	56.92	17.96	13.85	28.46	38.08	48.46	21.43	14.67	32.07	45.65	59.24	24.11
St23	18.10	34.48	42.24	45.69	21.22	41.54	74.23	85.00	92.31	56.31	31.92	55.38	66.54	78.08	43.01	31.52	53.80	66.85	78.80	42.49
St123	19.83	31.90	43.10	51.72	22.61	46.54	76.54	85.38	91.92	59.69	34.23	56.54	70.77	78.85	45.62	31.52	57.07	67.39	80.98	42.92

Table 6. Aerial-to-Aerial Re-ID results in AG-VPReID.VIR.

Method	RGB \rightarrow IR					IR \rightarrow RGB				
	R1	R5	R10	R20	mAP	R1	R5	R10	R20	mAP
St1	17.82	30.46	42.53	62.07	26.26	8.05	21.26	29.89	40.80	15.95
St2	25.86	47.13	58.05	74.14	37.26	11.49	28.16	33.91	43.10	19.69
St3	8.05	30.46	38.51	51.15	18.85	6.90	12.07	18.39	27.59	10.99
St12	30.46	56.90	66.09	77.01	42.40	20.69	39.66	50.57	56.90	29.89
St13	20.11	38.51	50.57	62.07	30.43	12.64	24.71	32.18	43.10	19.28
St23	31.61	54.02	63.22	75.86	43.17	20.11	31.61	43.10	49.43	26.93
St123	33.91	56.32	64.37	76.44	44.72	21.84	40.80	53.45	56.90	30.92

V2I. These represent substantial improvements over previous best methods—SAADG (13.07%/18.75%), AuxNet (15.70%/16.46%), and CST (14.23%/19.37%)—with absolute gains of 20.48-23.11% in Rank-1 and 22.19-25.10% in mAP for I2V. The performance gap is even more pronounced for V2I, where our approach outperforms the best competitors by 33.69-35.11% in Rank-1 and 37.18-39.07% in mAP. Notably, all methods experience dramatic performance drops when transitioning to AG-VPReID.VIR’s

cross-platform setting. While SAADG’s Rank-1 accuracy plummets from 69.22% to 13.07% (56.15% relative drop) and MITML falls from 63.74% to 12.16% (51.58% drop), our method maintains higher performance across datasets.

5.4. Ablation Study

We analyze the contribution of each component in our TCC-VPReID framework. Streams are denoted as St1 (Style-Robust Feature Learning), St2 (Memory-based Cross-View Adaptation), and St3 (Intermediary-Guided Temporal Learning). Results are in Tab. 5 and Tab. 6.

Individual Stream Performance. St2 consistently outperforms other individual streams (11.21% Rank-1 for Aerial \rightarrow Ground I2V, 40.38% for V2I), demonstrating temporal memory’s effectiveness for cross-domain challenges. St1 performs second-best, highlighting style-invariant features’ importance, while St3 performs lowest individually.

Combined Streams. The St12 combination significantly improves performance over individual streams (15.52% Rank-1 for Aerial \rightarrow Ground I2V vs. 11.21% for St2 alone).

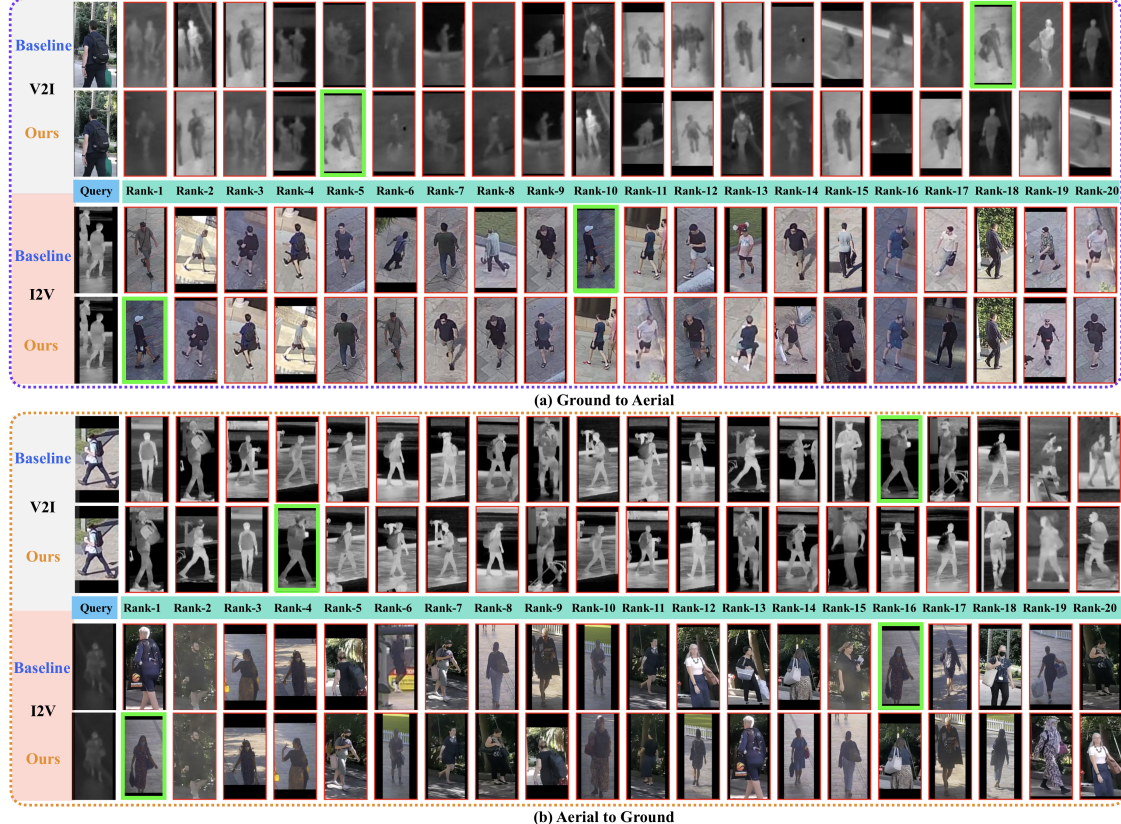


Figure 5. Visualization of top-20 ranking results on AG-VPReID.VIR dataset under aerial-ground cross-platform settings for I2V and V2I queries (I: infrared, V: visible). Red bounding boxes indicate incorrect matches, green indicate correct matches.

The full three-stream model (St123) achieves best overall results, confirming the complementary contributions of each stream.

Modality Direction Asymmetry. Performance significantly differs between V2I and I2V directions, with Aerial→Ground showing 46.54% vs. 19.83% Rank-1. This asymmetry suggests infrared queries face greater challenges when searching visible galleries, likely due to information loss in thermal imagery.

Platform Comparison. Same-platform cross-modality retrieval (33.91% Rank-1 for Aerial→Aerial RGB→IR) outperforms cross-platform scenarios (19.83% for Aerial→Ground I2V), quantifying the challenge of cross-platform variations beyond modality differences. The same observation can be made for Ground→Ground. Additional cross-platform results detailed in Table 7.

5.5. Qualitative Results

Fig. 5 compares our TCC-VPReID approach with the baseline [51] across cross-platform cross-modality settings. Results show significant ranking improvements in all scenarios (*e.g.* aerial-IR to ground-RGB from rank-16 to rank-1), confirming that our three-stream architecture effectively

Table 7. Performance comparison on AG-VPReID.VIR ground-to-ground vs. aerial-to-ground scenarios (infrared-to-visible).

Method	Ground→Ground R1 mAP	Aerial→Ground R1 mAP
MITML [CVPR'22]	12.16	16.93
SAADG [ACM MM'23]	13.07	18.75
CST [TMM'24]	14.23	19.37
Ours	36.18	41.56
		19.83
		22.61

tackles variations in viewpoint and modality.

6. Conclusion

We introduce AG-VPReID.VIR, the first comprehensive dataset for video-based cross-modality person re-identification across aerial and ground platforms, with 4,861 tracklets from 1,837 identities. Our proposed TCC-VPReID framework effectively tackles viewpoint variations and modality discrepancies through style-robust feature learning, memory-based cross-view adaptation, and intermediary-guided temporal learning. Experimental results show TCC-VPReID outperforms state-of-the-art methods by over 20% in both Rank-1 accuracy and mAP, setting a new challenging benchmark for robust cross-platform surveillance systems.

References

[1] G. C. Bertocco, F. Andaló, and A. Rocha. Unsupervised and self-adaptative techniques for cross-domain person re-identification. *IEEE Transactions on Information Forensics and Security*, 16:4419–4434, 2021.

[2] C. Chen, M. Ye, M. Qi, J. Wu, J. Jiang, and C.-W. Lin. Structure-aware positional transformer for visible-infrared person re-identification. *IEEE Transactions on Image Processing*, 31:2352–2364, 2022.

[3] D. Chung, K. Tahboub, and E. J. Delp. A two stream siamese convolutional neural network for person re-identification. In *ICCV*, pages 1983–1991, 2017.

[4] P. Dai, R. Ji, H. Wang, Q. Wu, and Y. Huang. Cross-modality person re-identification with generative adversarial training. In *IJCAI*, volume 1, page 6, 2018.

[5] M. Dreuw and ORB-HD. deface: Video anonymization by face detection, 2023. Python package version 1.5.0.

[6] Y. Du, C. Lei, Z. Zhao, Y. Dong, and F. Su. Video-based visible-infrared person re-identification with auxiliary samples. *IEEE Transactions on Information Forensics and Security*, 19:1313–1325, 2023.

[7] C. Eom, G. Lee, J. Lee, and B. Ham. Video-based person re-identification with spatial and temporal memory networks. In *ICCV*, pages 12036–12045, 2021.

[8] J. Feng, A. Wu, and W.-S. Zheng. Shape-erased feature learning for visible-infrared person re-identification. In *Proceedings of the IEEE/CVF conference on computer vision and pattern recognition*, pages 22752–22761, 2023.

[9] Y. Feng, F. Chen, J. Yu, Y. Ji, F. Wu, T. Liu, S. Liu, X.-Y. Jing, and J. Luo. Cross-modality spatial-temporal transformer for video-based visible-infrared person re-identification. *IEEE Transactions on Multimedia*, 26:6582–6594, 2024.

[10] X. Gu, H. Chang, B. Ma, H. Zhang, and X. Chen. Appearance-preserving 3d convolution for video-based person re-identification. In *ECCV*, pages 228–243. Springer, 2020.

[11] K. He, X. Zhang, S. Ren, and J. Sun. Deep residual learning for image recognition. In *Proceedings of the IEEE conference on computer vision and pattern recognition*, pages 770–778, 2016.

[12] R. Hou, H. Chang, B. Ma, S. Shan, and X. Chen. Temporal complementary learning for video person re-identification. In *Computer Vision–ECCV 2020: 16th European Conference, Glasgow, UK, August 23–28, 2020, Proceedings, Part XXV 16*, pages 388–405. Springer, 2020.

[13] G. Jocher, Ayush, and J. Qiu. Ultralytics YOLO. <https://github.com/ultralytics/ultralytics>, 2024. Accessed: 2024-03-22.

[14] H. Li, M. Liu, Z. Hu, F. Nie, and Z. Yu. Intermediary-guided bidirectional spatial-temporal aggregation network for video-based visible-infrared person re-identification. *IEEE Transactions on Circuits and Systems for Video Technology*, 33(9):4962–4972, 2023.

[15] J. Li, S. Zhang, and T. Huang. Multi-scale 3d convolution network for video based person re-identification. In *AAAI*, volume 33, pages 8618–8625, 2019.

[16] Z. Li, W. Liu, X. Chang, L. Yao, M. Prakash, and H. Zhang. Domain-aware unsupervised cross-dataset person re-identification. In *Advanced Data Mining and Applications*, 2019.

[17] S. Liao, Y. Hu, X. Zhu, and S. Z. Li. Person re-identification by local maximal occurrence representation and metric learning. In *CVPR*, pages 2197–2206, 2015.

[18] X. Lin, J. Li, Z. Ma, H. Li, S. Li, K. Xu, G. Lu, and D. Zhang. Learning modal-invariant and temporal-memory for video-based visible-infrared person re-identification. In *Proceedings of the IEEE/CVF Conference on Computer Vision and Pattern Recognition*, pages 20973–20982, 2022.

[19] H. Liu, X. Tan, and X. Zhou. Parameter sharing exploration and hetero-center triplet loss for visible-thermal person re-identification. *IEEE Transactions on Multimedia*, 23:4414–4425, 2020.

[20] W. Liu, X. Chang, L. Chen, D. Q. Phung, X. Zhang, Y. Yang, and A. G. Hauptmann. Pair-based uncertainty and diversity promoting early active learning for person re-identification. *ACM Transactions on Intelligent Systems and Technology (TIST)*, 11:1–15, 2020.

[21] Y. Liu, Z. Yuan, W. Zhou, and H. Li. Spatial and temporal mutual promotion for video-based person re-identification. In *AAAI*, volume 33, pages 8786–8793, 2019.

[22] N. McLaughlin, J. M. Del Rincon, and P. Miller. Recurrent convolutional network for video-based person re-identification. In *CVPR*, pages 1325–1334, 2016.

[23] D. T. Nguyen, H. G. Hong, K. W. Kim, and K. R. Park. Person recognition system based on a combination of body images from visible light and thermal cameras. *Sensors*, 17(3):605, 2017.

[24] H. Nguyen, K. Nguyen, S. Sridharan, and C. Fookes. Aerial-ground person re-id. In *2023 IEEE International Conference on Multimedia and Expo (ICME)*, pages 2585–2590. IEEE, 2023.

[25] H. Nguyen, K. Nguyen, S. Sridharan, and C. Fookes. Ag-reid. v2: Bridging aerial and ground views for person re-identification. *IEEE Transactions on Information Forensics and Security*, 2024.

[26] K. Nguyen, C. Fookes, S. Sridharan, F. Liu, X. Liu, A. Ross, D. Michalski, H. Nguyen, D. Deb, M. Kothari, et al. Ag-reid 2023: Aerial-ground person re-identification challenge results. In *2023 IEEE International Joint Conference on Biometrics (IJCB)*, pages 1–10. IEEE, 2023.

[27] H. Park, S. Lee, J. Lee, and B. Ham. Learning by aligning: Visible-infrared person re-identification using cross-modal correspondences. In *Proceedings of the IEEE/CVF international conference on computer vision*, pages 12046–12055, 2021.

[28] A. Radford, J. W. Kim, C. Hallacy, A. Ramesh, G. Goh, S. Agarwal, G. Sastry, A. Askell, P. Mishkin, J. Clark, et al. Learning transferable visual models from natural language supervision. In *International Conference on Machine Learning*, pages 8748–8763. PMLR, 2021.

[29] X. Tian, Z. Zhang, S. Lin, Y. Qu, Y. Xie, and L. Ma. Farewell to mutual information: Variational distillation for cross-modal person re-identification. In *Proceedings of*

the IEEE/CVF Conference on Computer Vision and Pattern Recognition, pages 1522–1531, 2021.

[30] A. Vaswani, N. Shazeer, N. Parmar, J. Uszkoreit, L. Jones, A. N. Gomez, Ł. Kaiser, and I. Polosukhin. Attention is all you need. In *Advances in Neural Information Processing Systems*, pages 5998–6008, 2017.

[31] G. Wang, T. Zhang, J. Cheng, S. Liu, Y. Yang, and Z. Hou. Rgb-infrared cross-modality person re-identification via joint pixel and feature alignment. In *ICCV*, pages 3623–3632, 2019.

[32] Z. Wang, Z. Wang, Y. Wu, J. Wang, and S. Satoh. Beyond intra-modality discrepancy: A comprehensive survey of heterogeneous person re-identification. In *International Joint Conference on Artificial Intelligence*, 2020.

[33] Z. Wang, Z. Wang, Y. Zheng, Y.-Y. Chuang, and S. Satoh. Learning to reduce dual-level discrepancy for infrared-visible person re-identification. In *CVPR*, pages 618–626, 2019.

[34] A. Wu, W.-S. Zheng, H.-X. Yu, S. Gong, and J. Lai. Rgb-infrared cross-modality person re-identification. In *Proceedings of the IEEE international conference on computer vision*, pages 5380–5389, 2017.

[35] J. Wu, L. He, W. Liu, Y. Yang, Z. Lei, T. Mei, and S. Z. Li. Cavit: Contextual alignment vision transformer for video object re-identification. In *European Conference on Computer Vision*, pages 549–566. Springer, 2022.

[36] Q. Wu, P. Dai, J. Chen, C.-W. Lin, Y. Wu, F. Huang, B. Zhong, and R. Ji. Discover cross-modality nuances for visible-infrared person re-identification. In *Proceedings of the IEEE/CVF conference on computer vision and pattern recognition*, pages 4330–4339, 2021.

[37] Y. Wu, Y. Lin, X. Dong, Y. Yan, W. Ouyang, and Y. Yang. Exploit the unknown gradually: One-shot video-based person re-identification by stepwise learning. In *Proceedings of the IEEE conference on computer vision and pattern recognition*, pages 5177–5186, 2018.

[38] S. Xu, Y. Cheng, K. Gu, Y. Yang, S. Chang, and P. Zhou. Jointly attentive spatial-temporal pooling networks for video-based person re-identification. In *ICCV*, pages 4733–4742, 2017.

[39] M. Yang, Z. Huang, P. Hu, T. Li, J. Lv, and X. Peng. Learning with twin noisy labels for visible-infrared person re-identification. In *Proceedings of the IEEE/CVF Conference on Computer Vision and Pattern Recognition*, pages 14308–14317, 2022.

[40] M. Ye, X. Lan, Q. Leng, and J. Shen. Cross-modality person re-identification via modality-aware collaborative ensemble learning. *IEEE Transactions on Image Processing*, 29:9387–9399, 2020.

[41] M. Ye, X. Lan, J. Li, and P. Yuen. Hierarchical discriminative learning for visible thermal person re-identification. In *Proceedings of the AAAI Conference on Artificial Intelligence*, volume 32, 2018.

[42] M. Ye, W. Ruan, B. Du, and M. Z. Shou. Channel augmented joint learning for visible-infrared recognition. In *Proceedings of the IEEE/CVF International Conference on Computer Vision*, pages 13567–13576, 2021.

[43] M. Ye, J. Shen, D. J. Crandall, L. Shao, and J. Luo. Dynamic dual-attentive aggregation learning for visible-infrared person re-identification. In *ECCV*, pages 229–247. Springer, 2020.

[44] M. Ye, J. Shen, G. Lin, T. Xiang, L. Shao, and S. C. H. Hoi. Deep learning for person re-identification: A survey and outlook. *IEEE transactions on pattern analysis and machine intelligence*, PP, 2021.

[45] C. Yu, X. Liu, Y. Wang, P. Zhang, and H. Lu. Tf-clip: Learning text-free clip for video-based person re-identification. In *Proceedings of the AAAI conference on artificial intelligence*, volume 38, pages 6764–6772, 2024.

[46] G. Zhang, H. Zhang, W. Lin, A. K. Chandran, and X. Jing. Camera contrast learning for unsupervised person re-identification. *IEEE Transactions on Circuits and Systems for Video Technology*, 33(8):4096–4107, 2023.

[47] S. Zhang, W. Luo, D. Cheng, Q. Yang, L. Ran, Y. Xing, and Y. Zhang. Cross-platform video person reid: A new benchmark dataset and adaptation approach. In *European Conference on Computer Vision (ECCV)*, 2024.

[48] Y. Zhang and H. Wang. Diverse embedding expansion network and low-light cross-modality benchmark for visible-infrared person re-identification. *arXiv preprint arXiv:2303.14481*, 2023.

[49] Y. Zhang, Y. Yan, Y. Lu, and H. Wang. Towards a unified middle modality learning for visible-infrared person re-identification. In *Proceedings of the 29th ACM International Conference on Multimedia*, pages 788–796, 2021.

[50] D. Zheng, J. Xiao, M. Sun, H. Bai, and J. Hou. Plausible proxy mining with credibility for unsupervised person re-identification. *IEEE Transactions on Circuits and Systems for Video Technology*, 33(7):3308–3318, 2022.

[51] C. Zhou, J. Li, H. Li, G. Lu, Y. Xu, and M. Zhang. Video-based visible-infrared person re-identification via style disturbance defense and dual interaction. In *Proceedings of the 31st ACM International Conference on Multimedia*, pages 46–55, 2023.

AG-VPReID.VIR: Bridging Aerial and Ground Platforms for Video-based Visible-Infrared Person Re-ID

Supplementary Material

7. Dataset Collection

Fig. 6 illustrates the strategic camera placement used for our AG-VPReID.VIR dataset collection across a university campus. The map highlights the diverse sensing infrastructure deployed to capture comprehensive cross-platform and cross-modality data: visible-only cameras (V), infrared-only cameras (IR), and dual-modality cameras capturing visible and infrared modalities simultaneously (VIR). We strategically positioned these cameras to maximize coverage while ensuring minimal overlap between different sensing modalities and viewing angles. The UAVs were deployed at fixed hovering positions (marked on the map) but at varying altitudes (15m, 25m, and 45m) to capture diverse aerial perspectives, while ground-based CCTV and wearable cameras provided complementary viewpoints. This comprehensive sensing network enabled the collection of synchronized multi-view data across different environmental conditions, creating challenging scenarios with varying illumination, occlusion, and viewing angles that closely mirror real-world surveillance scenarios.

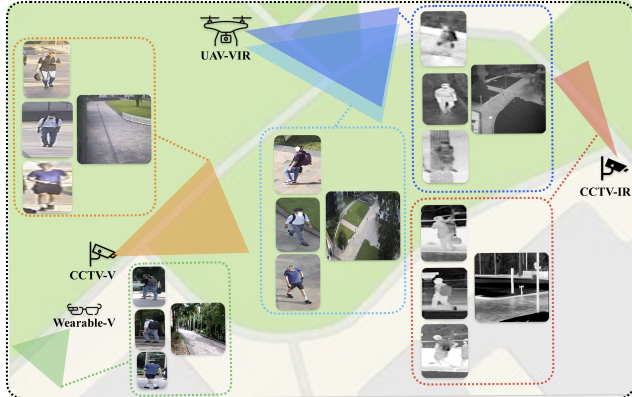


Figure 6. Data collection map. V denotes visible, IR means infrared, and VIR stands for both visible and infrared cameras.

8. Dataset Distribution Analysis

Fig. 7 illustrates the distribution of data across different camera types and modalities in our AG-VPReID.VIR dataset. The distribution shows a deliberate balance between RGB and IR modalities while maintaining diversity across platforms. UAV RGB contributes the largest portion (29.2%) of the dataset, providing rich aerial visible-light perspectives, while CCTV IR represents the second largest share (25.6%), offering extensive ground-level ther-

mal imagery. The complementary nature of CCTV RGB (18.9%), UAV IR (11.5%), and wearable RGB (14.8%) ensures comprehensive coverage across all deployment scenarios. This balanced distribution is critical for training robust cross-modality cross-platform Re-ID models, as it provides sufficient examples for the algorithm to learn the distinctive characteristics of each viewpoint-modality combination, particularly the challenging aerial IR perspective that is unique to our dataset.

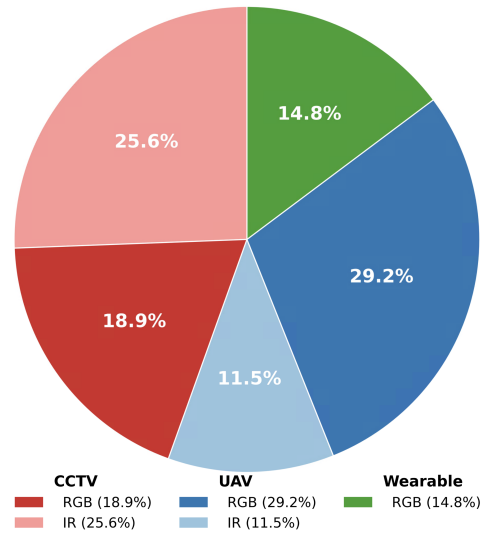


Figure 7. Distribution of identity presence across different camera types and modalities (RGB and IR) in our AG-VPReID.VIR dataset.

9. Challenges Addressed and Key Components of streams in the proposed architecture

Table 8 presents the comprehensive architecture of our TCC-VPReID framework, detailing how each stream addresses specific challenges in aerial-ground visible-infrared person re-identification. The three complementary streams work in concert to overcome the complex variations encountered in cross-platform cross-modality scenarios. Stream 1 focuses on style-robust feature learning to handle intra/inter-modal variations, frame-level style variations, and appearance distortions across platforms through components like style augmentation, cross-view graph interaction, and domain-adversarial alignment. Stream 2 addresses temporal and cross-view challenges through memory-based adaptation, constructing platform-specific memories that maintain identity consistency across aerial and ground per-

Table 8. Overview of TCC-VPReID: A Three-Stream Architecture for Cross-Platform Cross-Modality Video-based Person Re-ID

Stream	Challenges Addressed	Key Components
Stream 1: Style-Robust Feature Learning	<ul style="list-style-type: none"> Intra/inter-modal variations Frame-level style variations Appearance distortions across platforms 	<ul style="list-style-type: none"> Style Augmentation & Disturbance Defense Cross-View & Cross-Modal Graph Interaction Domain-Adversarial Alignment
Stream 2: Temporal Memory Adaptation	<ul style="list-style-type: none"> Aerial-ground viewpoint variations Temporal misalignment in sequences Unstable motion patterns across platforms 	<ul style="list-style-type: none"> Cross-View Memory Construction Transformer-Based Video Encoder Temporal Memory Diffusion
Stream 3: Modality-Invariant Representation	<ul style="list-style-type: none"> Modality gap (visible vs. infrared) Noisy frames in aerial/ground videos Information asymmetry between modalities 	<ul style="list-style-type: none"> Anaglyph-based Modality Bridging Bidirectional Spatial-Temporal Aggregation Modality Decoupling
Feature Fusion	<ul style="list-style-type: none"> Preserving complementary information Reconciling cross-platform/modality features Balancing spatial, temporal, and modality cues 	<ul style="list-style-type: none"> Multi-level Feature Integration Cross-stream Knowledge Transfer Joint Optimization Framework

spectives. Stream 3 targets the fundamental modality gap between RGB and IR imagery using anaglyph-based intermediary learning and bidirectional aggregation. These streams are integrated through a feature fusion module that preserves complementary information while reconciling contradictions across platforms and modalities. This multi-stream approach enables our framework to effectively disentangle the entangled variations in appearance, viewpoint, and modality that characterize aerial-ground visible-infrared person Re-ID.

10. Hyperparameter Ablation Study

We conducted ablation studies to determine the optimal values for the loss function hyperparameters (λ_1 , λ_2 , λ_3 , and λ_4). Tab. 9 shows the performance of our model with different hyperparameter configurations on the Aerial→Ground I2V protocol, which is one of the most challenging scenarios in our dataset.

Table 9. Ablation study on hyperparameters λ_1 , λ_2 , λ_3 , and λ_4 using Aerial→Ground I2V performance.

λ_1	λ_2	λ_3	λ_4	Rank-1	mAP
0.5	1.0	0.5	1.0	15.21	18.43
0.5	1.0	1.0	1.5	17.46	20.12
0.5	1.5	1.0	1.5	18.32	21.05
1.0	1.0	1.0	1.0	17.65	20.33
1.0	1.5	0.5	1.5	18.75	21.42
1.0	1.5	1.0	1.5	19.83	22.61
1.0	2.0	1.0	1.5	19.12	21.98
1.5	1.5	1.0	1.5	18.96	21.75
1.0	1.5	1.5	1.5	18.54	21.30
1.0	1.5	1.0	2.0	19.07	21.83

As shown in Tab. 9, we found that setting $\lambda_1 = 1.0$, $\lambda_2 = 1.5$, $\lambda_3 = 1.0$, and $\lambda_4 = 1.5$ achieves the best performance on our most challenging retrieval scenario. The results demonstrate that:

- The triplet loss (λ_1) performs best at a moderate weight of 1.0, balancing its contribution with other losses.
- The style attack loss (λ_2) benefits from a higher weight of 1.5, emphasizing the importance of style-invariant features for cross-platform scenarios.
- The cross-reconstruction loss (λ_3) is most effective at a moderate weight of 1.0, helping bridge modality gaps without overpowering other components.
- The video-to-memory contrastive loss (λ_4) performs optimally at 1.5, indicating the significance of temporal memory for cross-view adaptation.

We observed that increasing λ_2 and λ_4 beyond 1.5 led to performance degradation, suggesting that over-emphasizing these components can disrupt the balance between different learning objectives.